Cyanobacterial clock, a stable phase oscillator with negligible intercellular coupling

M. Amdaoud, M. Vallade, C. Weiss-Schaber, and I. Mihalcescu*

Laboratoire de Spectrométrie Physique, Centre National de la Recherche Scientifique Unité Mixte de Recherche 5588, Université Joseph Fourier–Grenoble I, BP 87, 38402 St. Martin d'Hères Cedex, France

Edited by Charles R. Cantor, Sequenom, Inc., San Diego, CA, and approved March 1, 2007 (received for review November 3, 2006)

Accuracy in cellular function has to be achieved despite random fluctuations (noise) in the concentrations of different molecular constituents inside and outside the cell. The circadian oscillator in cyanobacteria is an example of resilience to noise. This resilience could be either the consequence of intercellular communication or the intrinsic property of the built-in biochemical network. Here we investigate the intercellular coupling hypothesis. A short theoretical depiction of interacting noisy phase oscillators, confirmed by numerical simulations, allows us to discriminate the effect of coupling from noise. Experimentally, by studying the phase of concurrent populations of different initial phases, we evaluate a very small upper limit of the intercellular coupling strength. In addition, *in situ* entrainment experiments confirm our ability to detect a coupling of the circadian oscillator to an external force and to describe explicitly the dynamic change of the mean phase. We demonstrate, therefore, that the cyanobacterial clock stability is a built-in property as the intercellular coupling effect is negligible.

biological clock | bioluminescence | dynamics | synechoccocus

The circadian clock is a self-sustaining biological oscillator that evolved in numerous organisms such as cyanobacteria, algae, fungi, plants, insects, and vertebrates to coordinate their metabolic and behavioral activities with the Earth's daily rotation (1). The free running period of the circadian clock is nearly, but not exactly, 24 h and is synchronized with the geophysical day by such periodic environmental cues as light, temperature, and nutrition. The molecular mechanism of the circadian rhythm production is generally described as a system of interlocked transcription/translation feedback loops (2).

Single cell *in vivo* monitoring revealed that individual cells generate autonomous circadian rhythms in protein abundance (3). In multicellular organisms, the individual cell rhythms appear to be noisy with drifting phases and frequencies (4, 5). Random fluctuations in the concentrations of different molecular constituents inside and outside the cell could be a cause of this noise (6). However, the whole organism is significantly more accurate, the temporal precision being achieved most probably through intercellular coupling of the individual noisy oscillators (7, 8).

In cyanobacteria, single cell oscillators are impressively stable, and a first estimation rules out strong intercellular coupling (9). Interestingly, these prokaryotes also have the simplest molecular mechanism at the heart of their circadian clock. In the absence of transcriptional activity *in vivo* (10), as well as alone *in vitro* (11), the three clock proteins KaiA, KaiB, and KaiC generate a self-sustained circadian oscillation of autophosphorylation and dephosphorylation. Recent chemical kinetics models (12, 13) provide a possible understanding of the three-protein oscillator, but the measured *in vivo* stability still remains unexplained. Do cyanobacteria possess not only the simplest circadian clock but also the most stable one? However, the same apparent stability could also be the result of weak intercellular coupling (14). The tendency for the individual phases of oscillation to drift away from each other could be overridden by an as-yet-unmeasured weak coupling. Is the clock stability a built-in property for each bacterium, or does a weak intercellular coupling make them appear like that?

Here we address this question by an accurate evaluation of the coupling constant. For that we first theoretically design our experiment to be able to distinguish coupling, even weak, from phase diffusion. As the precision of our evaluation increases with the length of the experiments, we continuously monitor, for a couple weeks, mixtures of cell populations with different initial phases. The inherent experimental noise contribution, initially dominant, is reduced by enhanced statistics. In the last section, we confirm our theoretical hypotheses and our experimental sensitivity by new experiments of *in situ* entrainment.

Model

The aim of this section is to show theoretically that when two populations with widely different abundances are mixed, the time evolution of the mean phase of the minority population will allow the coupling between bacteria to be measured directly.

Because single cell experiments (9) have previously ruled out a strong coupling between circadian clocks in cyanobacteria, we consider only the weak coupling limit. The cyanobacterial oscillators are taken to be phase oscillators (with constant amplitudes), and the interaction between two oscillators is described by the first Fourier term, i.e., the sine of the difference of the two oscillator phases (15). These assumptions will be experimentally confirmed afterward. Theoretical, numerical (15, 16) as well experimental (17) studies confirm that phase models can capture important synchronization properties of populations with weak interactions. This tremendous simplification of the oscillator complex dynamics exploits the fact that for a weak coupling, the amplitude variation or fluctuation can be separated from the slow phase change driven by the weak coupling and slight frequency differences among the oscillators (15).

The phase dynamics of two interacting oscillators is then given by

$$\frac{d\phi_j}{dt} = \omega_j + \varepsilon \sin(\phi_k - \phi_j), \qquad [1]$$

where $\phi_j(t)$ is the instantaneous phase of the oscillator, ω_j is its free-running frequency, and ε is the coupling constant.

Population of *N* Identical, Weakly Coupled, Noisy Oscillators. The cyanobacterial oscillators are also submitted to noise. We discriminate here between two types of noise: the first, experimental, is generated by global environmental fluctuations or manual interventions such as addition of medium (see *Materials and Methods*). This affects all oscillators in roughly the same way and

Author contributions: M.V. and I.M. designed research; M.A., M.V., C.W.-S., and I.M. performed research; M.A., C.W.-S., and I.M. analyzed data; and I.M. wrote the paper.

The authors declare no conflict of interest.

This article is a PNAS Direct Submission.

*To whom correspondence should be addressed. E-mail: irina.mihalcescu@ujf-grenoble.fr.

This article contains supporting information online at www.pnas.org/cgi/content/full/0609315104/DC1.

will not be taken into account in this section. A second type of noise, specific to each oscillator, comes from the stochastic nature of chemical reactions inside each cell. This can in principle affect the phase, as well as the free-running frequency or the shape of the oscillation. For a given experimental condition, single cell experiments showed a closely similar period of oscillation for all of the cells studied (standard deviation/mean $<$ 0.5%). We therefore consider identical oscillators with the same free running frequency ω_0 and the stochastic noise affecting only the phase of the oscillation in a generic Wiener process. For N identical mutually coupled oscillators, Eq. **1** becomes the Kuramoto equation (16), here represented in a ω_0-rotating frame with $\varphi = \phi - \omega_0 t$:

$$\frac{d\varphi_j}{dt} = \frac{\varepsilon}{N}\sum_{k=1}^{N}\sin(\varphi_k - \varphi_j) + \xi_j(t). \qquad [2]$$

The noise terms $\xi_j(t)$ are independent stochastic Gaussian functions with zero mean and diffusion constant D, δ-correlated in time: $\langle\xi_i(t)\xi_j(t')\rangle = D\delta(t - t')\delta_{ij}$. In our experiments, the number N of identical oscillators is large, $N > 10^6$.

Let $P(\varphi, t)$ be the probability of observing a given bacterium with phase φ at time t. The time progress of $P(\varphi, t)$ is given by the solution of the corresponding Fokker–Planck equation (18):

$$\frac{\partial P(\varphi,t)}{\partial t} = \varepsilon\frac{\partial}{\partial\varphi}[(X\sin\varphi - Y\cos\varphi)P(\varphi,t)] + \frac{D}{2}\cdot\frac{\partial^2 P(\varphi,t)}{\partial\varphi^2}, \qquad [3]$$

where X, Y are the real and imaginary part of the mean field

$$Z = X + iY = \frac{1}{N}\sum_{k=1}^{N} e^{i\varphi_k} = \frac{1}{2\pi}\int_{-\pi}^{\pi} P(\varphi, t)e^{i\varphi}d\varphi.$$

Note that the amplitude ρ of the mean field $Z = \rho e^{i\mu}$ is the order parameter, a direct measure of the synchronization: for oscillators uniformly distributed $\rho = 0$, whereas $\rho = 1$ when all oscillators have exactly the same phase. The steady-state solution [see supporting information (SI)] of Eq. **3** is the von Mises (19) distribution:

$$P(\varphi) = \frac{1}{2\pi I_0(k)}e^{k\cos(\varphi-\mu)},$$

the circular analogue of the normal distribution on a line. Here $\mu \in [-\pi, \pi)$ is the mean phase, k is a parameter bi-univocally related to the order parameter $\rho = I_1(k)/I_0(k)$, and $I_n(k)$ is the modified Bessel function of the first kind of order n. The self-consistency condition ensuing from Eq. **3** $\rho_s = I_1(k_s)/I_0(k_s) = (D/\varepsilon)\cdot(k_s/2)$ gives (SI) that the only steady-state solution is the uniform distribution of phases for $D > \varepsilon$, when the noise prevails, whereas partial synchronization is achieved for $\varepsilon > D$.

Mixture of Two Imbalanced Populations of Identical Noisy Oscillators. In our experiment we mix two populations of oscillators, a first one denoted as "majority" has a number of oscillators N_M much larger than N_m, the number of oscillators in the second, "minority" population ($N_M/N_m = 20$). Being entrained in the same way (see *Materials and Methods*), both populations have initially identical phase distributions ($\rho_M^0 = \rho_m^0$), albeit centered around different averages, μ_M^0 and μ_m^0, respectively. If the coupling strength ε is strong enough compared with D, one would expect that the mean phase of the minority population would drift toward that of the majority population.

To derive an analytical solution for the time evolution of the phase distributions in both populations we make two main approximations (see SI): (*i*) we assume that the attractive force acting on all oscillators comes mainly from the majority population; (*ii*) we approximate the probability densities $P_M(\varphi, t)$ for the majority and $P_m(\varphi, t)$ for the minority population by von Mises distributions at any time point. In fact, initially and at steady state, $P_M(\varphi, t)$ and $P_m(\varphi, t)$ are von Mises distributions (see SI), and we subsequently interpolate between these two limits. With these approximations, the time-dependent parameters $\mu_M(t)$, $\rho_M(t)$, and $\mu_m(t)$, $\rho_m(t)$, which characterize the time progression of the two populations, are given by (SI)

$$\begin{aligned}\frac{\partial\rho_M}{\partial(\varepsilon t)} &= \frac{\rho_M}{2}\cdot\left(\frac{2\rho_M}{k_M} - \frac{D}{\varepsilon}\right)\\ \frac{\partial\rho_m}{\partial(\varepsilon t)} &= \frac{\rho_m}{2}\cdot\left[\frac{2\rho_M}{k_m}\cdot\cos(\mu_M - \mu_m) - \frac{D}{\varepsilon}\right]\\ \frac{\partial\mu_m}{\partial(\varepsilon t)} &= \frac{\rho_M}{\rho_m}\cdot\left(1 - \frac{\rho_m}{k_m}\right)\cdot\sin(\mu_M - \mu_m),\end{aligned} \qquad [4]$$

and $\mu_M(t) = \mu_M^0$. In Eqs. **4**, εt appears as the natural reduced time. Consequently, excluding the initial conditions, the ratio D/ε remains the only parameter affecting the evolution of the minority mean phase $\mu_m(\varepsilon t)$ and both order parameters $\rho_M(\varepsilon t)$ and $\rho_m(\varepsilon t)$. Fig. 1 compares the numerical simulation of Eq. **2**, for different values of ε and D/ε, with the solution of Eqs. **4**. The good agreement validates our previous approximations, in the parameter range of our experimental circumstances.

It is remarkable that the influence of D/ε on $\mu_m(\varepsilon t)$ is weak: Fig. 1*a Inset* shows similar variation of $\mu_m(\varepsilon t)$ for D/ε values, from 0.01 to 10. For $\varepsilon t \ll 1$, $\mu_m(t)$ is independent of the diffusion coefficient value D, whereas $\rho_M(t)$ and $\rho_m(t)$ depend strongly on D:

$$\begin{aligned}\mu_m(t) - \mu_m^0 &\cong (1 - \rho_0/k_0)\cdot\sin(\mu_M^0 - \mu_m^0)\cdot\varepsilon t\\ \rho_M(t) &\cong \rho_0[1 + (\varepsilon\rho_0/k_0 - D/2)\cdot t]\\ \rho_m(t) &\cong \rho_0[1 + (\varepsilon\rho_0/k_0\cdot\cos(\mu_M^0 - \mu_m^0) - D/2)\cdot t].\end{aligned} \qquad [5]$$

We can therefore evaluate the coupling constant ε, independently of D. The appropriate physical measure is the slope of the time progression of the minority mean phase, $\mu_m(t)$. Because the precision in the estimation of the slope increases with monitoring time, our experiments are designed to follow $\mu_m(t)$ for a couple weeks continuously.

Experimental Results

We follow the temporal progression of the mean phase of the minority population by using the strain AMC462. This strain is bioluminescent, carrying a bacterial luciferase reporter that consists of two neutral site chromosomal insertions, *PkaiBC*::*luxAB* and *PpsbAI*::*luxCDE*. Although the clock is ticking in the same way as in a wild-type (WT) strain, the reporter inserted here makes it possible to observe the oscillations. The large difference in population abundance excludes the use of two color bioluminescence reporters (20), one for each population of the mixture, owing to the spectral leakage of the majority reporter signal into that of the minority. To avoid any loss of the minority signal by a 20-fold more abundant majority, we therefore use for the majority population the WT strain with no reporter, i.e., nonbioluminescent. Note that the white-light illumination of 900 lux provides each cell with at least 10^7 more photons than the bioluminescent reporter (see SI). This excludes any feedback influence of the bioluminescent light on the bacterial clock.

Both strains were similarly entrained, $\rho_M^0 = \rho_m^0 = \rho_0$, at independent initial mean phases (see *Materials and Methods*) μ_m^0 and μ_M^0. We chose to work with four initial phases, denoted A,

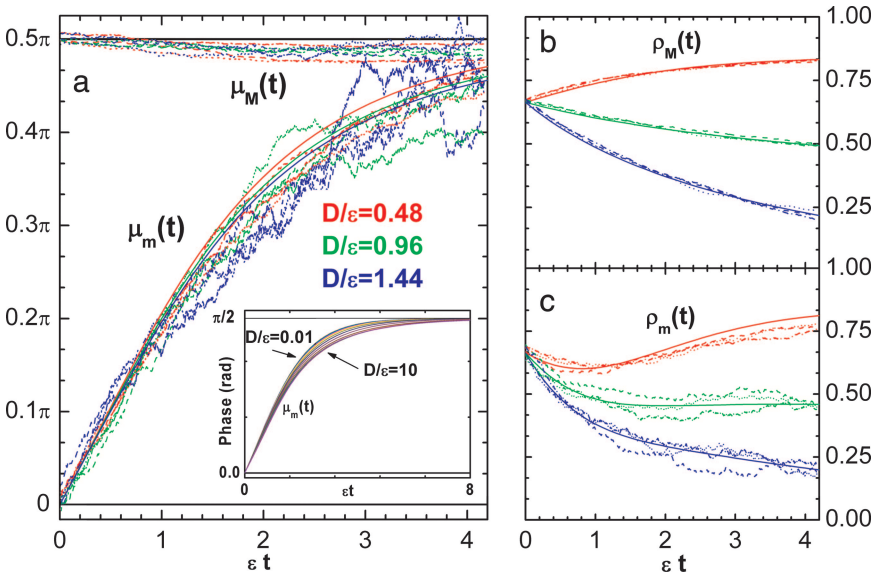

Fig. 1. Comparison between the solution of Eqs. **4** (solid line) and numerical simulations of 10,500 interacting phase oscillators. The mean phases $\mu_M(\varepsilon t)$ and $\mu_m(\varepsilon t)$ (*a*), order parameter of the majority population $\rho_M(\varepsilon t)$ (*b*), and order parameter of the minority population $\rho_m(\varepsilon t)$ (*c*) are represented for three values of D/ε, 0.48 (red line), 0.96 (green line), and 1.44 (blue line). Three simulations are superimposed for each value of D/ε, with different values of the coupling constant: $\varepsilon = 0.2$ (dashed line), 0.1 (dash-dot line), and 0.05 (dotted line). (*a Inset*) Similar variation of $\mu_m(\varepsilon t)$, obtained from Eqs. **4** for D/ε varying from 0.01 to 10.

B, C, and D, separated by $\cong\pi/2$ rad (Fig. 2*a Inset*). Mixtures were made in 96-well plates, for different pairs, (μ_m^0, μ_M^0): from (a, A), (a, B) . . . to (d, C) and (d, D). Lowercase denotes mean phases of the minority and uppercase those of the majority population.

***In Situ* Monitoring of the Relative Minority/Majority Concentration by Using the Bioluminescence Baseline.** Fig. 2*a* presents the bioluminescence recorded from individual wells containing mixtures of the same minority with four different majorities: (a, A), (a, B), (a, C), and (a, D), followed for ≈40 days. As a control, we also observe the luminescent strain alone, here shown for two initial mean phases A and C. For each well, the bioluminescence $i(t)$ oscillates around a baseline $\overline{i(t)}$ that, apart from a weekly brief rise when fresh medium is added, gradually decreases all along the experiment. $\overline{i(t)}$ is the temporal mean calculated by smoothing the bioluminescence curve. The baseline value depends on the number of cells per well. At low cell numbers the well is transparent and the bioluminescence, collected from the whole well, is proportional to the absolute number of emitters. For higher concentrations of cells per well, as described in *Materials and Methods*, detection of the luminescence is confined only to the top layers of cells, and $\overline{i(t)}$ is proportional to the relative concentration of emitters/total number of cells in a well (see SI). We use this property to monitor the relative minority/majority population concentration. Fig. 2*a* shows that, initially, the wells containing the luminescent strain alone indeed emit ≅20 times more strongly than the mixtures. In time, the WT strain outgrows the reporter strain, which enhances even further the ratio between minority and majority abundance: $N_m/N_M \cong 1/30$.

Experimental Monitoring of the Minority Mean Phase. Fig. 2 *b* and *c* illustrates the circadian oscillation, $s(t)$, for the same wells and individual time points as in Fig. 2*a*. The sensitivity of the bioluminescence reporter to the metabolic conditions is circumvented by defining the oscillatory signal as $s(t) = i(t)/\overline{i(t)} - 1$. This representation reveals a remarkable well-to-well reproducibility of the oscillations. The wells containing the luminescent strain alone maintain their phase opposition until the end of the experiment (Fig. 2*b*). The oscillation of the minority population appears to be unperturbed by the majority presence: throughout the experiment, their oscillations overlap regardless of the majority mean phase (Fig. 2*c*).

It can be shown that $s(t)$ is in fact proportional to the real part of mean field Z_m of the detected oscillators in the well. For this, we express the bioluminescence of the cell j as $d_j(t) = g\cdot[1 + b\cos(\omega_0 t + \varphi_j)]$, where ω_0 and φ_j are the free running frequency and the phase of the oscillator j, respectively. g is the reporter gain, and b is the relative amplitude of oscillation per cell. The latter depends on the promoter monitored, here *PkaiBC*. Initially, $b \cong 1$, then decreases during the experiment, depending on the metabolic state of the cell (see SI). The well bioluminescence is the sum of the contribution of all of the top cells and is therefore proportional to their ensemble average oscillation, $i(t) \propto \langle d(t)\rangle$ (see SI), which finally gives: $s(t) = b\rho\cos(\omega_0 t + \mu)$. The time variation of the amplitude $b\rho$ describes the apparent damping of $s(t)$ oscillations in Fig. 2 *b* and *c*. Because b is time dependent, variable from one experiment to another, and accounts for nearly all of the amplitude damping, it is not possible to get a reliable experimental determination of $\rho(t)$ for a quantitative comparison with the theoretical expectations (Eq. **5**). By contrast, the phase of $s(t)$ is precisely the mean phase μ, and for this reason we will employ this quantity to monitor the minority mean phase.

The Hilbert Transform is used to construct the complex analytical signal associated with the oscillation $s(t)$ and to extract the instantaneous phase (see SI). Fig. 2*d* follows the temporal progression of the minority phase $\mu_m(t)$ for individual wells containing mixtures of the same minority with four different majorities: (a, A), (a, B), (a, C), and (a, D), shown in Fig. 2*a*. In our representation, the reference is $\langle\mu_{(a,A)}(t)\rangle$, the average of wells containing a mixture with the same initial phase (see *Materials and Methods*) $\mu_m^0 = \mu_M^0 = A$. Theoretically, in the other mixtures, where $\mu_m^0 \neq \mu_M^0$, we would expect the minority to drift gradually toward the phase of the majority (Fig. 1*a*), if the coupling is strong enough. Fig. 2*d*, however, shows no apparent phase deviation. The instantaneous phases spread out around zero, in a similar way to reference mixture (a, A) wells. We may conclude either that there is no intercellular interaction between oscillators or, more likely, that the experimental noise causing this dispersion masks a possible weak coupling.

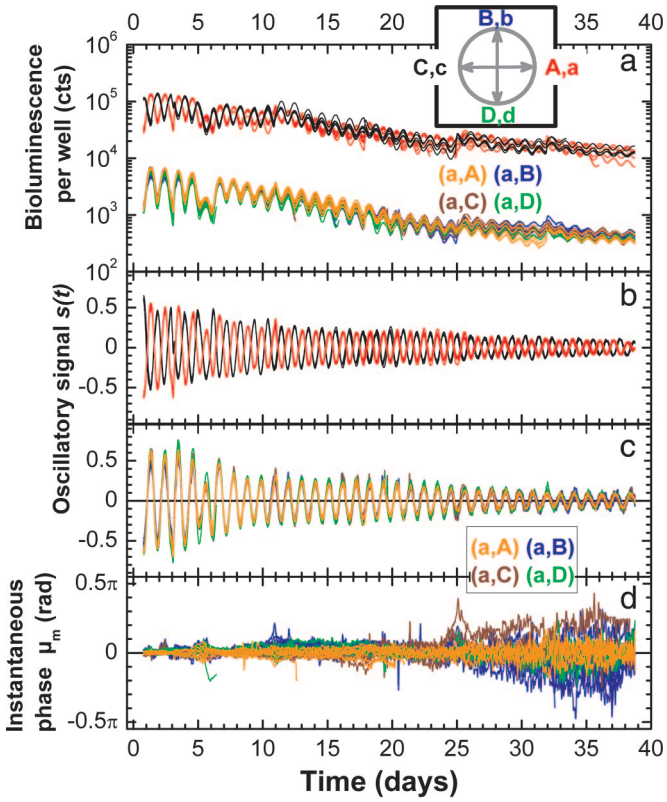

Fig. 2. The mean phase of the minority population is unaffected by the presence of a different phase majority. (*a*) Recorded bioluminescence of individual wells. Red and black lines indicate wells containing only luminescent cells previously entrained at opposite phases (A and C, respectively). Orange, blue, brown, and green lines represent wells containing mixtures of a luminescent minority with a 20 times larger population of WT cells as follows: (a, A), (a, B), (a, C), and (a, D). Lowercase denotes minority and uppercase indicates majority mean phase. The mixtures have a bioluminescence level initially 20 times and finally 30 times lower than wells containing only the luminescent strain. Each experimental condition is represented by 8–12 independent wells. (*Inset*) The four phases of entrainment are separated by $\cong\pi/2$ rad, with A leading B, in opposition to C and lagging D. (*b* and *c*) The circadian oscillation $s(t)$ for the luminescent strain alone (*b*) and for the mixtures (*c*), represented with the same colors as in *a*. $s(t) = i(t)/\overline{i(t)} - 1$, with $i(t)$ the well bioluminescence and $\overline{i(t)}$ its baseline obtained by a fast Fourier transform (FFT) smoothing of $i(t)$. The oscillations of A and C still have opposite phases at the end of the experiment. For the mixtures, the oscillation of the minorities appears unbiased by the presence of different phase majorities. (*d*) Instantaneous mean phase of the minorities $\mu_m(t)$ extracted from $s(t)$, represented with the same colors as in *a*.

Estimation of the Intercellular Coupling. To extract from the experimental noise a possible minority phase variation, we average the individual well contributions from all of the measurements. The average is taken over equivalent experiments, i.e., wells with the same initial phase difference $\mu_M^0 - \mu_m^0$ between majority and minority. As described previously, the reference for each well is its corresponding average of same-phase mixtures $\mu_m^0 = \mu_M^0$. Fig. 3 compares the variation of the average minority phase $\langle\mu_m(t)\rangle$ for three initial differences of phase: $-\pi/2$, π, $\pi/2$. Here again the minority phase variation is buried in the remaining noise and exhibits a similar variation for all three conditions. We therefore stop our quest to uncover an intercellular coupling. The precision of our experiment, however, enables us to set an upper limit for this elusive coupling constant ε.

To this end we use Eq. **5**, because the condition $\varepsilon t \ll 1$ is obviously valid. The expected variation of the minority phase is linear, with the slope directly related to ε: $(1 - \rho_0/k_0)\cdot\varepsilon\cdot\sin(\mu_M^0 - \mu_m^0)$. Here the initial order parameter (see *Materials and Methods*) is $\rho_0 \cong 0.67$ and $k_0 = 1.8$. The extreme scenario is for $\mu_M^0 - \mu_m^0 = \pm\pi/2$, where we would have expected the strongest variation of the minority mean phase. Fig. 3 shows the 95% confidence bands of the simultaneous linear fit (see SI) of both $\pm\pi/2$ curves. The resulting 95% confidence interval confines the coupling constant ε to a value of $|\varepsilon| < 1.5{\cdot}10^{-3}$ day^{-1}. It follows that, even in the absence of noise, it would take at least 500 days, or $\approx$1 year, for the minority to join the majority. As will be shown in the next section, variations in the natural environmental are so large over such an extended period that this value of ε amounts in practical terms to zero.

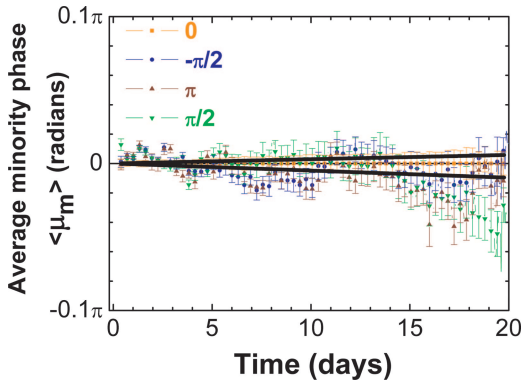

Fig. 3. The average minority phase $\langle\mu_m(t)\rangle$ for three initial phase differences $\mu_M^0 - \mu_m^0$: $= -\pi/2$, π, $\pi/2$ and the reference 0, represented, respectively, by blue, brown, green, and orange lines (error bars are the standard error of the mean). For each phase, the average is taken over $\cong$80 individual wells. Black lines show 95% lower and upper confidence limits of the linked linear fit of the $\pm\pi/2$ curves.

External Force Acting on a Population of *N* Identical, Noisy Oscillators. In this last section we analyzed a simpler coupling experiment. An external force, here the external lighting, is coupled to a population of identical noisy oscillators, the cyanobacteria. This experiment was designed to evaluate our ability to detect coupling and also as a quantitative test of the coupling model considered above (Eq. 1).

A particular lighting signal in front of each well (see *Materials and Methods*), $E_j(t) = E_0{\cdot}[1 + c_j{\cdot}\cos(\omega t + \theta_{0j})]$ is applied to a plated population of freshly entrained luminescent cells. The average applied light intensity $\overline{E(t)} = E_0$ and frequency ω are the same for all of the wells, whereas, from well to well, the relative amplitude of the oscillatory component c_j and the initial phase θ_{0j} are varied (Fig. 4*a*). A 1-day (24 h) entrainment period is imposed and four different entrainment phases, separated by $\pi/2$. The entrainment frequency ω is chosen to be different from ω_0 (free running frequency of the oscillator) for two reasons. First, the entrainment to a 24-h period is one of the three defining circadian clock properties and is thus a guarantee that coupling exists and can be studied. Second, a strictly resonant coupling ($\omega = \omega_0$) is trickier to impose, because the free running frequency of the oscillators $\omega_0(t)$ changes slightly in time. We denote the detuning, $\nu = \omega - \omega_0$, such that $\nu > 0$, because the cyanobacterial circadian oscillators period is >24 h.

The time-response of the oscillator mean phase $\mu_j(t)$ to the entrainment signal $E_j(t)$ is then monitored. Fig. 4*b* shows the average phase variation $\langle\mu(t)\rangle$ relative to the initial phase μ_0, represented in a ω-rotating frame. In this representation, the instantaneous phase of a free running oscillator (of constant ω_0) decreases linearly with a slope $-\nu$, whereas it is constant for an oscillator locked at the entrainment frequency. In our case (Fig. 4*b*), the average phases start from the same point (origin) and,

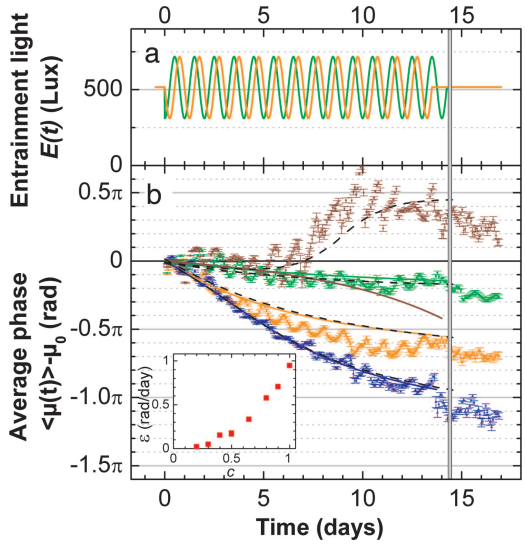

Fig. 4. Cyanobacterian oscillators respond to an external force as phase oscillators. (*a*) Entrainment lighting $E(t)$ is applied for ≅14 days and then kept constant for the next 3 days to confirm the phase change. The light oscillates around an average of 500 lux, with a relative amplitude $c = 0.4$ and a 24-h period. Two of the four entrainment phases, separated by $\pi/2$, are shown. The gray vertical line highlights the transition to constant lighting. (*b*) The phase of the related entrained oscillators represented in a ω-rotating frame. The orange, green, blue, and brown symbols and error bars correspond to the experimental average phase $\langle\mu(t)\rangle - \mu_0$ and standard error of the mean; the matching colored lines are the fits from the Adler equation with ε the only free parameter. Dashed black lines are the numerical simulations of Eq. **6**, with the same ε. (*Inset*) The coupling constant ε increases with the relative amplitude of entrainment c.

under the influence of entrainment, evolve toward the $\pi/2$ separated phases. These phase differences persist when the entrainment is stopped, for $t > 14$ days.

We can go one step further and quantify the coupling constant ε involved here. We adopt the same assumption as in Eq. **1**, except that now, instead of two oscillators, there is an entrainment force of instantaneous phase $\theta_e(t) = \omega t + \theta_0$, coupled to an oscillator of instantaneous phase $\phi_j(t)$. In the ω-rotating frame the equation becomes $d\phi_j/dt = -\nu - \varepsilon \sin[\phi_j - \Delta\theta]$, where $\Delta\theta = \theta_0 - \phi_0$ is the entrainment and oscillator difference of the initial phases. This equation, known as the Adler equation, has an analytic solution that depends on ε, ν, and $\Delta\theta$ (SI): for $\varepsilon > \nu$, the oscillator finally adopts the entrainment frequency, whereas for $\varepsilon < \nu$, the phase rotates nonuniformly in a quasiperiodic motion (15). In Fig. 4*b*, the continuous lines show the simultaneous fit of the experimental curves with this solution, with $\varepsilon = 0.15$ day^{-1} as the only free parameter. $\Delta\theta$ differs by steps of $\pi/2$ from one curve to another and ν, the same for all, is determined from the continuously illuminated wells (data not shown). As can be seen, three of the four curves are well described by this simplified model. For the fourth (brown) curve, the discrepancy with the experimental data is obvious: the average phase jumps up toward $\pi/2$, while the theoretical solution slowly decreases toward $-3\pi/2$. This is not surprising because our oversimplified model neglects the initial phase distribution ($\sigma_0 = 0.9$ rad) and the phase diffusion noise $\xi_j(t)$ (9). We therefore simulate (see *Materials and Methods*), for each oscillator j of the initial distribution, the equation

$$\frac{d\phi_j}{dt} = -\nu - \varepsilon \sin[\phi_j - \Delta\theta] + \xi_j(t), \qquad [6]$$

where ε has the value previously obtained. The resulting mean phases, represented in Fig. 4*b* by the dashed curves, now describe satisfactorily all of the experimental results.

Our experimental setup therefore allows us to detect and interpret coupling. The phase oscillator model is appropriate and provides an explicit description of the dynamic change of the mean phase. The relative amplitude of the oscillatory component c manifests itself as the strength of the entrainment force. For different values of $c \in (0, 1]$, the corresponding coupling coefficient ε steadily increases with c and vanishes for $c \leq 0.2$ (Fig. 4 *Inset*).

The above experiment also probes the sensitivity of the cyanobacterial circadian clock to an external perturbation. The circadian clock appears to be quite rigid, because relative amplitudes of >50% are necessary to produce locked 24-h light entrainment.

Discussion

In situ light entrainment experiments confirm that the cyanobacterian clock responds like a classical noisy phase oscillator to small entrainment forces. In a population of identical mutually coupled noisy oscillators, the steady-state distribution of phases relies on the comparative values of the phase diffusion constant D and the coupling constant ε. If $\varepsilon > D$, the coupling is stronger, and the phases can be driven toward a distribution of limited width. In contrast, if the noise is stronger ($D > \varepsilon$), the phases ultimately are uniformly distributed between $[-\pi, \pi)$. As a result, the outcome of apparent precision of oscillators also will depend on the ranking of D with respect to ε. Earlier single cell experiments (9) revealed robust circadian oscillators in cyanobacteria with a low phase diffusion $D = 5 \times 10^{-4} \pm 3 \times 10^{-4}$ h^{-1} $= 0.012 \pm 0.007$ day^{-1}. The estimated upper limit of ε excluded a strong coupling, $\varepsilon \leq 0.008\omega_0 = 0.05$ day^{-1} (see the supplementary information in ref. 9) but was too high to allow a direct comparison with D. Here, we have reduced the upper limit of the coupling constant by a factor of 30 to $|\varepsilon| \leq 0.0015$ day^{-1}. We show that the circadian clock in cyanobacteria therefore is dominated by a very low diffusion, because the coupling constant is even smaller.

The high stability of individual oscillators in cyanobacteria is therefore not related to intercellular coupling but originates from the internal wiring of the genetic and metabolic network. Their clock mechanism is not only the simplest but also the most robust. The cyanobacterial circadian oscillator appears as a simple model system for studying dynamic noise-resistant networks. What makes this oscillator noise resistant? The posttranslational core of the clock, based on the repeated interaction of the three clock proteins Kai A, B, and C is potentially less noisy than a transcription/translation clock mechanism (6). Is that enough to explain the cyanobacterian clock stability or are supplementary transcription/translation feedback loops needed to obtain this stability? Cyanobacteria offer two complementary approaches for answering this question: first, *in vivo* single cell experiments, by decoupling the core clock from the existent feedback loops, and, second, reverse engineering *in vitro* by microscale reconstituted clocks with the similar number of proteins as *in vivo*.

Materials and Methods

Strains, Growth Conditions, and Entrainment. The strains used in this study are AMC 462 (21) and WT *Synechoccocus* sp. strain PCC 7942. Strain AMC462 carries a luciferase reporter, consisting in two neutral site chromosomal insertions *PkaiBC*::*luxAB* and *PsbAI*::*luxCDE*. Both strains were grown in modified BG-11 medium (22) at 30°C in a CO_2-controlled atmosphere and 900-lux white-lamp illumination. The phases of the cultures were set the same by light-entrainment, 12-h light/12-h dark cycles during 1 week. The two strains were then frozen

in cryotubes with 150 $\mu l \cdot ml^{-1}$ glycerol at $-80°C$. Freezing cyanobacteria stops the circadian clock ticking, whereas thawing them restarts it. Therefore, to obtain samples with exactly the same oscillation characteristics but different mean phases, cryotubes were thawed at different time intervals, diluted, and kept in constant conditions of light, temperature, and CO_2. The phase difference is directly related to the time interval Δt between each thawing: $\Delta\varphi = 2\pi\Delta t/T$, where T is the circadian clock period. In this way we obtained cell cultures with the desired mean phase and the same distribution of individual cell phases around this mean. The standard deviation of this distribution was concordantly evaluated to $\sigma_0 = 0.9$ rad from individual cell measurements (results not shown) and from the initial amplitude of the oscillatory signal $s(t = 0)$. This corresponds (SI) to an order parameter $\rho_0 \cong 0.67$ and to a concentration parameter $k_0 = 1.8$.

***In Situ* Light Entrainment.** In the coupling with an external force experiment, we built two arrays of 96 individual white-light emitting diodes (LED), their size matching the plates. The LED arrays were designed to avoid cross-illumination of wells, in such a way that one LED illuminated exactly one well. A custom-made program varied the LED light emission, independently for six clusters per plate, each cluster containing 4×4 LEDs. In these experiments, a sinusoidal light signal was applied, with the same 24-h period and 500 lux average light intensity for all of the clusters but with different initial phases and amplitudes of oscillation.

Assay of Bioluminescence. A Packard Topcount 96-well plate luminescence reader was used to follow the circadian oscillations of the luminescent strain. Each well of the 96-well plate was filled with the same amount of cells, 250 μl at an optical density measured at 750 nm, $OD_{750nm} \approx 0.1$, that is $\approx 3 \times 10^7$cells per well. The plates then were covered with adhesive sealing film, perforated above each well to ensure the presence of oxygen and CO_2 inside the wells. Two plates were placed in a room regulated for temperature (30°C) and CO_2 under constant white light (900 lux), to avoid any unwanted external entrainment. Every 30 min, the luminescence of each well was automatically read by two photomultipliers under darkness for 5 sec per well, i.e., 4 min per plate. Before each reading, the plates were kept in darkness for 2 min. To compensate for evaporation and nutrient depletion, fresh media was added every week to the wells.

During the experiment, the number of cells in the wells continued to grow: color photographs of the plates were taken every week showing the wells becoming greener because of the increasing chlorophyll concentration. This growth rapidly confined detection of the luminescence only to the top layers of cells, because the green-colored cyanobacteria reabsorbed the bioluminescence photons emitted by the bottom layers (see SI). In addition, the nutrient resources shared among increasingly numerous members will reduce the gain of the biochemical luminescent reaction per cell. Therefore, except for the first few days and for a weekly brief rise when fresh medium was added, the bioluminescence gradually decreased all throughout the experiment. We detected the same number of top cells, and they were emitting less. For each experimental condition, we started with 8–16 independent wells, some of which were excluded from our analysis on account of contamination, too fast evaporation, or clogged aeration of the cover film. The exclusion criterion used was the variation of the bioluminescence baseline by >40% with respect to an unperturbed well.

Numerical Simulations and Circular Statistical Analysis. We numerically integrated the evolution of phases for 10,500 interacting phase oscillators governed by Eq. **2**, by using a forward Euler scheme with time step $\Delta t = 2.6 \times 10^{-3}$. The initial phase of the oscillators, independently distributed, has one majority group of $N_{maj} = 10{,}000$, normally distributed around $\mu_M^0 = \pi/2$ and one minority group of $N_{min} = 500$ normally distributed around $\mu_m^0 = 0$. Initially, both groups have the same standard deviation, $\sigma_0 = 0.9$ rad. The noise ξ, a Wiener process with a diffusion constant D, is simulated by a phase jump $\xi = \pm\sqrt{D\Delta t}$ that is equally probable forward or backward at each time step. The same technique is used in the simpler case of coupling with an external force. We simulated Eq. **6** for 2,000 oscillators, initially independently distributed around 0, with the standard deviation $\sigma_0 = 0.9$ rad.

Interpretation of the results was done by using the circular analysis statistics (23). The mean order parameter $\langle\rho\rangle$ and the mean phase $\langle\mu\rangle$ were determined as follows:

$$\langle\rho\rangle = \frac{1}{N}\sqrt{\left(\sum_{i=1}^{N}\cos\varphi_i\right)^2 + \left(\sum_{i=1}^{N}\sin\varphi_i\right)^2}$$

$$\text{and } \tan\langle\mu\rangle = \sum_{i=1}^{N}\sin\varphi_i \Big/ \sum_{i=1}^{N}\cos\,\varphi_i.$$

In this paper, the time average of a random variable $x(t)$ is denoted by $\bar{x}$ and the ensemble average by $\langle x(t)\rangle$.

We thank B. Houchmandzadeh and E. Geissler for discussions and comments on the manuscript and P. Ballet, J. Giraud, and S. Rochat for advice and technical assistance. This work was supported in part by an Action Concerteé "Dynamique et réactivité des assemblages biologiques" and a Contrat de Plan État-Région (CPER) "Nouvelles Approches Physiques des Sciences du Vivant."

1. Foster G, Kreitzman L (2004) *Rhythms of Life* (Profile, London).
2. Bell-Pedersen D, Cassone VM, Earnest DJ, Golden SS, Hardin PE, Thomas TL, Zoran MJ (2005) *Nat Rev Genet* 6:544–556.
3. Nagoshi E, Saini C, Bauer C, Laroche T, Naef F, Schibler U (2004) *Cell* 119:693–705.
4. Welsh DK, Yoo SH, Liu AC, Takahashi JS, Kay SA (2004) *Curr Biol* 14:2289–2295.
5. Carr AJ, Whitmore D (2005) *Nat Cell Biol* 7:319–321.
6. Raser JM, O'Shea EK (2005) *Science* 309:2010–2013.
7. Liu C, Weaver DR, Strogatz SH, Reppert SM (1997) *Cell* 91:855–860.
8. Herzog ED, Aton SJ, Numano R, Sakaki Y, Tei H (2004) *J Biol Rhythms* 19:35–46.
9. Mihalcescu I, Hsing W, Leibler S (2004) *Nature* 430:81–85.
10. Tomita J, Nakajima M, Kondo T, Iwasaki H (2005) *Science* 307:251–254.
11. Nakajima M, Imai K, Ito H, Nishiwaki T, Murayama Y, Iwasaki H, Oyama T, Kondo T (2005) *Science* 308:414–415.
12. Emberly E, Wingreen NS (2006) *Phys Rev Lett* 96:038303.
13. Mehra A, Hong CI, Shi M, Loros JJ, Dunlap JC, Ruoff P (2006) *PLoS Comput Biol* 2:e96.
14. Njus D, Gooch VD, Hastings JW (1981) *Cell Biophys* 3:223–231.
15. Pikovsky A, Rosenblum M, Kurths J (2001) *Synchronization: A Universal Concept in Nonlinear Science* (Cambridge Univ Press, Cambridge, UK).
16. Strogatz SH (2000) *Physica D* 143:1–20.
17. Kiss IZ, Zhai Y, Hudson JL (2005) *Phys Rev Lett* 94:248301.
18. Gardiner CW (1985) *Handbook of Stochastic Methods for Physics, Chemistry and the Natural Sciences* (Springer, Berlin).
19. von Mises R (1918) *Phys Z* 19:490–500.
20. Kitayama Y, Kondo T, Nakahira Y, Nishimura H, Ohmiya Y, Oyama T (2004) *Plant Cell Physiol* 45:109–113.
21. Katayama M, Tsinoremas NF, Kondo T, Golden SS (1999) *J Bacteriol* 181:3516–3524.
22. Bustos SA, Golden SS (1991) *J Bacteriol* 173:7525–7533.
23. Mardia KV, Jupp PE, (1999) *Directional Statistics*, Wiley Series in Probability and Statistics (Wiley, New York).